JBC RESEARCH ARTICLE

Physcomitrium patens flavodiiron proteins form heterotetrametric complexes

Received for publication, February 6, 2024, and in revised form, July 11, 2024 Published, Papers in Press, August 8, 2024,
https://doi.org/10.1016/j.jbc.2024.107643

Claudia Beraldo[1], Eleonora Traverso[1], Marco Boschin[1], Laura Cendron[1], Tomas Morosinotto[1], and Alessandro Alboresi[1,2,*]

From the [1]Department of Biology, University of Padova, Padova, Italy; [2]National Biodiversity Future Center, Università degli Studi di Palermo, Palermo, Italy

Reviewed by members of the JBC Editorial Board. Edited by Joseph Jez

Flavodiiron proteins (FLVs) catalyze the reduction of oxygen to water by using electrons from Photosystem I (PSI). In several photosynthetic organisms such as cyanobacteria, green algae, mosses and gymnosperms, FLV-dependent electron flow protects PSI from over-reduction and consequent damage especially under fluctuating light conditions. In this work we investigated biochemical and structural properties of FLVA and FLVB from the model moss *Physcomitrium patens*. The two proteins, expressed and purified from *Escherichia coli*, bind both iron and flavin cofactors and show NAD(P)H oxidase activity as well as oxygen reductase capacities. Moreover, the co-expression of both FLVA and FLVB, coupled to a tandem affinity purification procedure with two different affinity tags, enabled the isolation of the stable and catalytically active FLVA/B hetero tetrameric protein complex with cooperative nature. The multimeric organization was shown to be stabilized by inter-subunit disulfide bonds. This investigation provides valuable new information on the biochemical properties of FLVs, with new insights into their *in vivo* activity.

Light is essential for photosynthesis, but when in excess it can damage the photosynthetic apparatus, leading to photo-oxidative stress. As soon as photosynthetic organisms are exposed to saturating light intensity, Photosystem I (PSI) and II (PSII) can suffer from the consequences of excess excitation pressure. PSII can be photodamaged (photoinhibition) by the production of reactive oxygen species formed *via* the interaction of oxygen (O_2) with the triplet excited state of chlorophyll (^{3}Chl). PSI can experience over-reduction due to an excessive flow of electrons causing inactivation of its iron-sulfur clusters and photoinhibition (1, 2). While there is an efficient repair mechanisms for PSII, the recovery from eventual damage to PSI requires resynthesis of the whole complex, a slow process that requires several days with a significant metabolic costs for the cell (2–4). Essential metabolic pathways, such as the Calvin-Benson cycle and photorespiration, along with cyclic and pseudo-cyclic electron flows support electron flow at the PSI acceptor side and contribute to avoiding over-reduction of PSI (5, 6). Pseudo-cyclic electron flow, also called water-water cycle, involves photosystem II (PSII) that removes electrons from water to produce O_2 and PSI to reduce O_2 back to water. Pseudo-cyclic electron flow is either sustained by the Mehler reaction or by the activity of flavodiiron proteins (FLVs), enzymes that function as "safety-valves" when linear electron transport though Ferredoxin-$NADP^+$-Reductase (FNR) and NADPH pool is saturated (7). FLVs were shown to be active during the induction of photosynthesis in different organisms such as cyanobacteria (8–10), the model microalga *Chlamydomonas reinhardtii* (11), the bryophytes *Marchantia polymorpha* (12) and *Physcomitrium patens* (13) and gymnosperms (14). FLV activity was shown to be particularly important to avoid over-reduction in organisms exposed to light fluctuations (10, 13).

Photosynthetic FLVs belong to a large family of flavodiiron proteins (usually shortened as FDPs), metalloenzymes that are widespread in Bacteria and Archaea and that catalyze O_2 or nitric oxide (NO) reduction. All FDPs have a modular architecture with two conserved core domains (15). At the N-terminus lies a conserved diiron center in a metallo-β-lactamase-like domain enabling electron transfer reactions crucial for O_2/NO reduction. This is followed by a flavodoxin domain, harboring a flavin mononucleotide (FMN). Apart from the two core domains, different FDPs present various extra modules (15). FLVs found in photosynthetic organisms are characterized by a NAD(P)H:flavin oxidoreductase domain at the C-terminus (16), providing each monomer with a putative electron entry site. The presence of this domain in the FLV sequence suggested that NADPH could be the electron donor for the reaction (17, 18), but *in vivo* spectroscopic studies identified reduced ferredoxin as the main electron donor to Flv1/3 for reducing O_2 to water in cyanobacteria (19). Consistently, in *C. reinhardtii* FLVs was shown to compete for electrons with [FeFe]-hydrogenases and this could be explained by the fact that both proteins use the same electron donor, ferredoxin (20). A crystal structure of Flv1 was recently obtained, but in a version lacking the specific NAD(P)H:flavin oxidoreductase domain (Flv1-ΔFlR) (21), so the structural and functional relationship of full-length FLVs remains elusive.

Multimeric organization of photosynthetic FLVs is a feature still to be fully clarified. Genes encoding for FLV are always found in couples (22, 23), and functional analysis of *flv* knock-

* For correspondence: Alessandro Alboresi, alessandro.alboresi@unipd.it.

out lines in different organisms suggested that FLVs are active as heterocomplexes. As an example for prokaryote photoautotrophs, *Synechocystis* strains impaired in either Flv1 or Flv3 showed a similar phenotype of higher PSI acceptor side limitation (8, 24) and significant growth defects under fluctuating light conditions (25). In red plastid lineage, coral symbionts of the family Symbiodiniaceae have a polycistronic locus expressing FLVA and FLVB in tandem in a single polypeptide that is cleaved by a post-translational mechanism (26). Similarly, eukaryotes of the green lineage such as green algae, and land plants like mosses and gymnosperms express two homologous proteins (FLVA and FLVB) (11–13). It was shown that in the moss *P. patens* the lack of one FLV proteins impairs the accumulation also of the other FLV protein, suggesting that one functional partner stabilizes the other (13). In this context the moss *P. patens* appeared to be an excellent model system for studying FLVs in land plants since these organisms hold an evolutionary key position between aquatic and subterrestrial life making it a suitable organism to study processes that allowed land colonization. Also, it is interesting to highlight that even though FLVs are absent in the group of angiosperms, FLVA/B of *P. patens* functioned when expressed in *Arabidopsis thaliana* (27) and in *Oryza sativa* (28). While biochemically FLVA/B were proposed to be heterotetramers based on native gel electrophoresis (27, 28), no *in vitro* studies managed to isolate FLVA/B or Flv1/3 (*Synechocystis* sp. PCC6803) interaction so far. To cover for the lack of biochemical information, in this study, we successfully established the first expression and purification of recombinant flavodiiron proteins from a eukaryotic photosynthetic organism. *P. patens* FLVA and FLVB purified from *Escherichia coli* were shown to bind iron and flavin and display NAD(P)H-dependent oxygen reductase activity. We isolated a functional FLVA/B heterocomplex that was shown to be stabilized by inter-molecular disulfide bridges.

Results

P. patens *flavodiiron protein sequence and structural prediction analysis*

To investigate the properties of plant FLVs, we aligned and analyzed the protein sequences of *P. patens* FLVA (723 *aa*) and FLVB (647 *aa*) (Fig. S1). They exhibited 34.68% identity with each other, in line with other members of the same family (29). Based on the amino acid sequence and domain annotation database, we identified the FLVA and FLVB metallo-β-lactamase domain (residues 119–310 for FLVA and 122–310 for FLVB), flavodoxin-like domain (residues 406–545 for FLVA and 340–474 for FLVB) and flavin reductase-like domain (residues 574–723 for FLVA and 498–646 for FLVB) (Figs. 1 and S1). FLVA showed specific additional residues (I^{313}-K^{364}) that are absent in FLVB and that likely form two α-helices connecting the metallo-β-lactamase-like domain and the flavodoxin-like domain. AlphaFold prediction of structures of both enzymes revealed a conserved modular three-domain composition, consistent with the sequence analysis (Fig. 1). Two domains of *P. patens* FLVs are conserved with other FDPs and therefore they share high similarity with the partial crystal structure of Flv1-ΔFlR protein from *Synechocystis* (21) that is a homologue of *P. patens* FLVA (23) (Fig. S2*A*). Alpha-fold provided additional prediction also for the C-terminal domains of FLVA and FLVB, which are flavin reductase-like typical of the FDPs found in photosynthetic organisms (Figs. 1 and S1).

Recombinant P. patens *flavodiiron proteins bind flavin and iron*

To characterize *P. patens* FLVs, the recombinant mature FLVA and FLVB were purified by affinity chromatography after heterologous expression in *E. coli*. A StrepII-tag and a 6xHis-tag were respectively fused at the N-terminal part of mature FLVA and FLVB deprived of the chloroplast target peptide. An excess of riboflavin and ammonium iron (II) sulfate was added to the bacterial culture to stimulate the incorporation of the co-factors. StrepII-Tag-FLVA and 6xHisTag-FLVB were expressed independently, and their expression and purification were validated through SDS-page and immunoblot analysis utilizing either antibodies targeting FLVA and Strep-Tag (Figs. 2*A* and S3*A*) or antibodies against FLVB and His-Tag (Figs. 2*B* and S3*B*). The UV-Vis absorption spectra of purified FLVA and FLVB displayed a primary peak at 280 nm and two additional absorption peaks at 373 nm and 450 nm, characteristic of protein binding to the flavin moiety (Fig. 2, *C* and *D*) demonstrating that FMN was bound to the purified protein. Quantification of FMN content by the analysis of the absorption spectra estimated that each monomer of FLVA and FLVB bound approximately one molecule of flavin per monomer (Table S1). This is consistent with protein sequence analysis demonstrating that both FLVA and FLVB possess typical flavin-binding residues in their sequences, including hydrophilic residues essential for orthophosphate recruitment, as well as aromatic residues (FLVA Ser_{412}-x-Tyr_{414}-xx-Asn_{416}x80-Ser_{496}-Phe_{497}-x-Trp_{498}, FLVB Ser_{346}-x-Tyr_{348}-xx-Ser_{351}x74-Ser_{425}-Phe_{426}) (Fig. S2*B*).

The presence of iron in the purified proteins was also assessed by a colorimetric ferrozine-based assay, that showed approximately 1:1 protein iron molar ratio (Fig. S4 and Table S1). Analysis of the amino acid residues highlighted a classical Asp/Glu/His pattern in FLVB (His_{167}-x-Glu_{169}-x-$Asp_{171}His_{172}$-x61-His_{234}-x18-Asp_{253}-x56-His_{310}) expected to coordinate the two iron ions of the catalytic site. In FLVA, a diiron binding site was also identified in the protein sequence but with peculiar, more basic, amino acid composition (His_{170}-x-Ser_{172}-x-Lys_{174}x70-Arg_{246}-x18-Lys_{265}-x-His_{375}).

P. patens *FLVs are active and catalyze a NAD(P)H-dependent oxygen reduction reaction*

Like all photosynthetic FLVs, *P. patens* FLVA and FLVB are characterized by a flavin reductase-like domain. To assess the activity of purified enzymes, we performed *in vitro* assays previously used to study other members of the FDP enzyme family (18, 30). In particular, we conducted a spectroscopic assay to explore the ability of recombinant FLVA and FLVB to

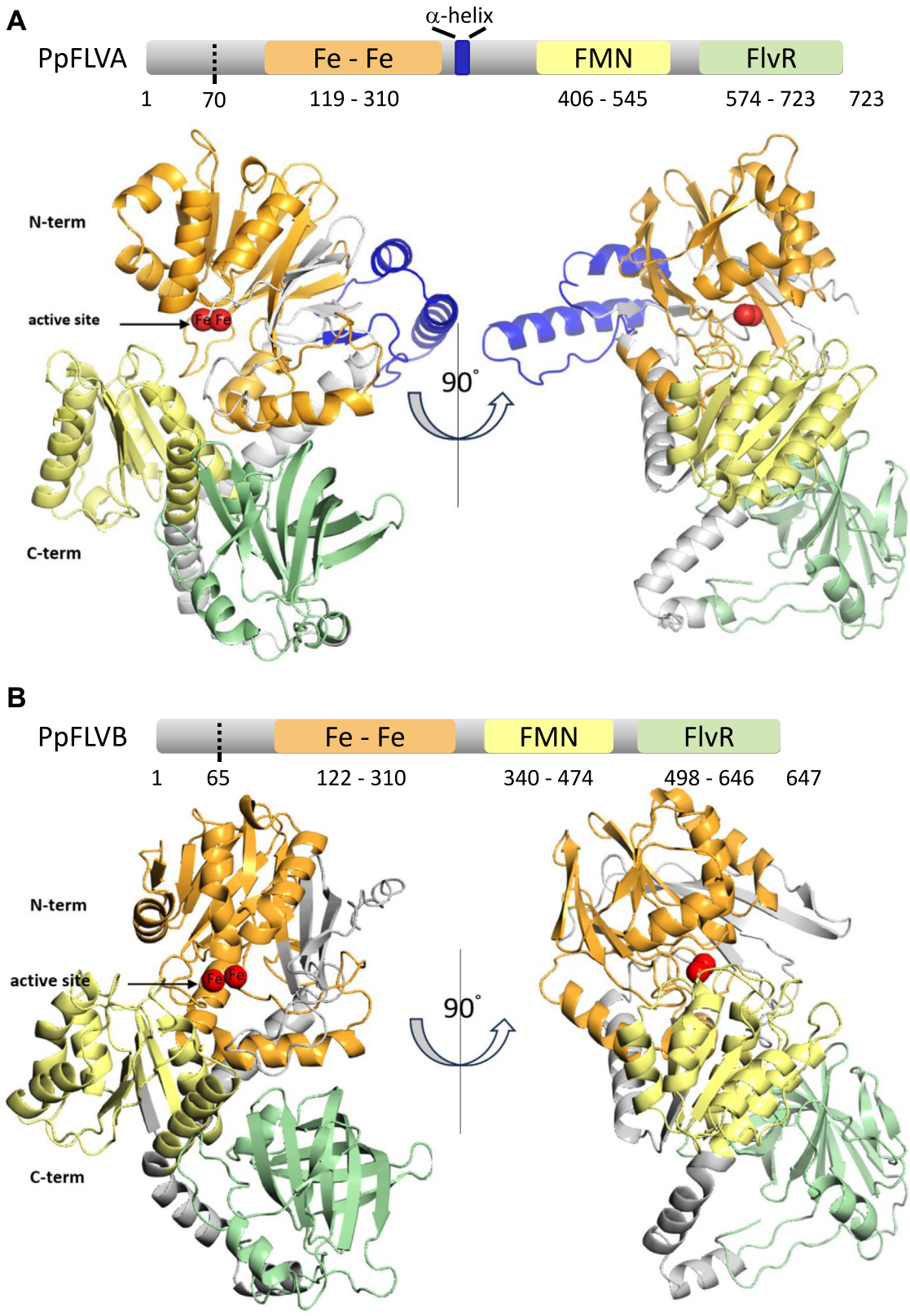

Figure 1. Predicted structure analysis of *Physcomitrium patens* FLVA and FLVB. *A*, schematic representation and AlphaFold model of FLVA (A9RYP3) and (*B*) FLVB (A9RQ00) structures. *Dotted lines* indicate the predicted cleavage sites for FLVA (position 70) and FLVB (position 65) chloroplast target peptides. The N-terminal metallo-β-lactamase domain contains a diiron center (Fe-Fe), the flavodoxin-like domain harbors a flavin mononucleotide (FMN), and the C-terminal domain is a flavin reductase-like domain (FlvR). The three domains are shown respectively in *orange*, yellow, and green. FLVA-specific residues (I^{313}-K^{364}) are shown in *blue*. Iron atoms (Fe) are represented as red spheres present in the active site.

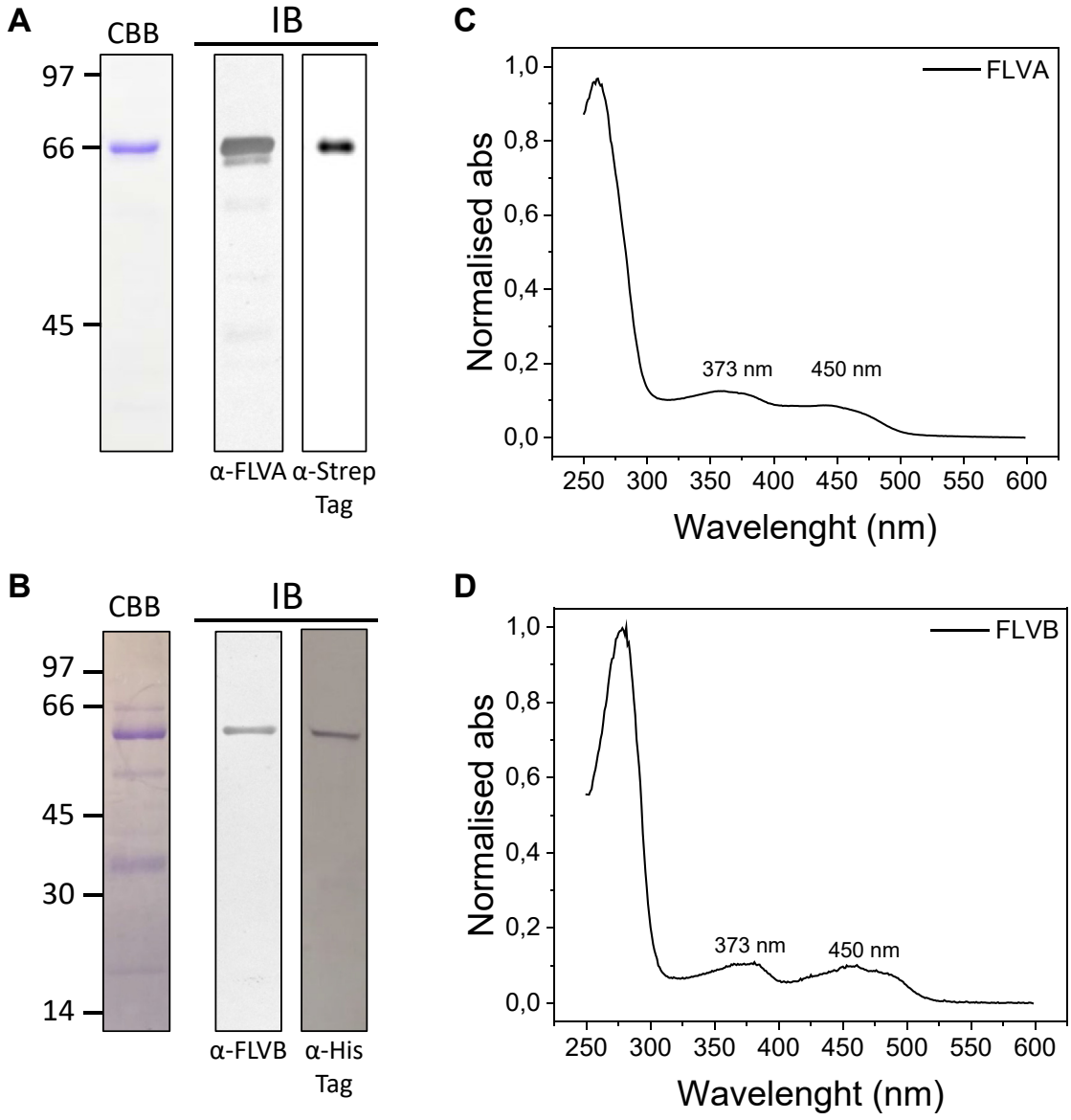

Figure 2. FLVA and FLVB biochemical properties. FLVA and FLVB biochemical properties. Coomassie Brilliant Blue-stained SDS-PAGE (CBB) of purified FLVA (*A*) and FLVB (*B*) and immunoblot analysis (IB) performed with antisera anti-FLVA and anti-Strep-Tag (*A*) and anti-FLVB and anti-His-Tag. On the left side, the apparent molecular weight of the ladder is reported in kDa. UV-visible absorption spectra of purified FLVA (*C*) and FLVB (*D*). Absorption spectra of approximately 5 μM protein in a solution containing 30 mM Tris and 300 mM NaCl at pH 8.0 were recorded at room temperature.

oxidize NADH and NADPH (Fig. 3), that was already shown to be effective for cyanobacterial FLVs (17, 18). NADH oxidation, monitored from OD_{340nm}, started as soon as FLVA and FLVB were added to the reaction solution, demonstrating that the isolated proteins were folded and active (Fig. 3*A*). The two enzymes were also able to oxidize NADPH (Fig. 3*B*). The kinetic parameters of the reactions were fitted to the steady state-Hill equation (Fig. 3, *C* and *D*). Both enzymes showed Hill coefficient>1 indicating cooperativity of NADH binding to the purified proteins. FLVA and FLVB showed similar affinity for NADH, K′ of 32 ± 6 and 41 ± 13 respectively), but FLVA showed a smaller turnover rate as compared to FLVB, with the latter isoform showing higher catalytic activity (Table 1).

In photosynthetic cells, FLVs perform O_2 reduction to water. To independently confirm the activity of purified proteins, we next assessed the capacity of recombinant *P. patens* FLVB to reduce O_2 using respirometry (Fig. 4). When FLVB was incubated in the measuring chamber, O_2 levels were stable until NADH was added, which caused a fast decrease in O_2 concentration, demonstrating that the protein indeed consumed O_2. When O_2 levels stabilized, a further addition of NADH resumed O_2 reduction reaction, indicating that the enzyme was stable over time and reaction stopped because of exhaustion of reducing power (Fig. 4). It is interesting to notice that O_2 consumption was fully FLV-dependent, because there was no effect of NADH addition to the measuring chamber simply containing measuring buffer (Fig. 4).

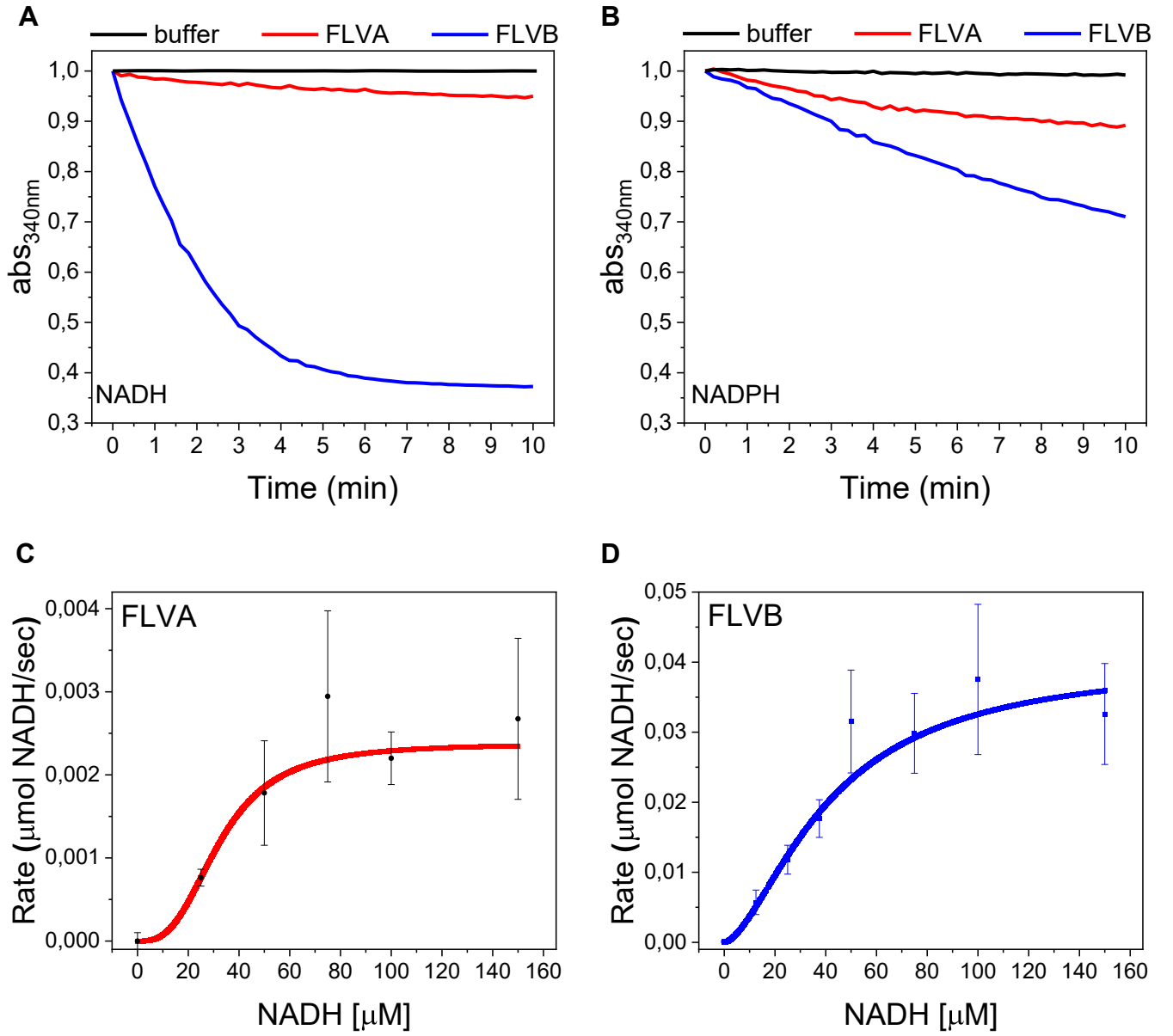

Figure 3. Kinetics of FLVA and FLVB NAD(P)H oxidase activity. FLVA and FLVB activity were tested in the presence of either 150 µM NADH (*A*) or NADPH (*B*). *Red lines* correspond to 7 µM FLVA and blue lines correspond to 7 µM FLVB. *Black lines* correspond to the negative control in the absence of FLV proteins. Traces were shifted to OD_{340nm} equal to 1 as a starting point immediately after FLV protein addition. Absorption spectra were recorded at room temperature. *C-D*, Hill fitting kinetics and fitted values for purified FLVA and FLVB in the presence of NADH. The *solid line* indicates Hill fitting curve of FLVA (*C*) or FLVB (*D*). n = 3 reactions were performed in the presence of FLVA and different concentrations of NADH, n = 4 reactions were performed in the presence of FLVB and different concentrations of NADH. Mean values are represented ± SEM.

FLVA and FLVB form stably bound and functional heterocomplex

FLVA and FLVB accumulation in *P. patens* needs the mutual presence of the two proteins since the depletion of one causes the destabilization of the other and the complete loss of FLV activity (13). Even though data suggest that FLVs are active together *in vivo*, an FLV heterocomplex has never been purified and characterized so far. To this aim, bacteria co-

Table 1
Hill kinetics of NADH oxidation for FLVA and FLVB

Purified protein	K' (µM NADH)	V_{max} (µM NADH* s^{-1})	n (Hill coefficient)
FLVA	32.38 ± 5.72	0.0023 ± 0.0002	2.89 ± 1.42
FLVB	41.34 ± 13.00	0.40 ± 0.01	1.61 ± 0.40

Values were obtained from fits to the steady-state Hill equation showed in Figure 3, *C* and *D*. Three independent biological replicates were performed, values are expressed ± standard deviation.

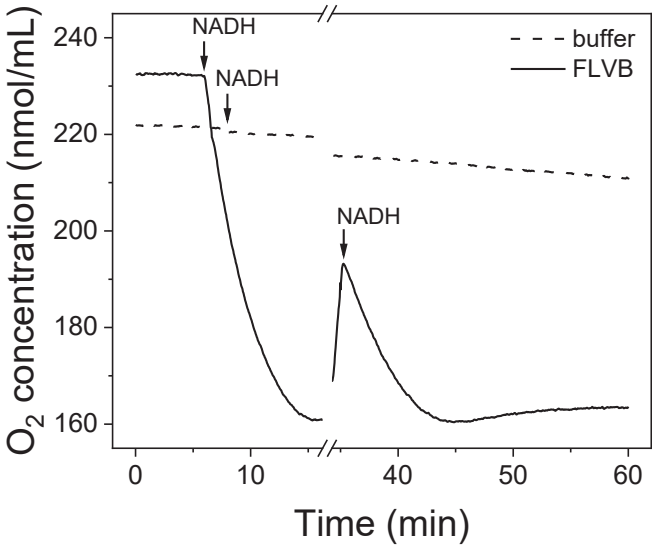

Figure 4. High-resolution respirometry of *P. patens FLVB* performed in an Oroboros Oxygraph-2k. The measurement started with sample buffer (Tris 30 mM and NaCl 300 mM) either containing 6 μM FLVB (*solid line*) or not (*dashed line*). After about 7.5 min 150 μM NADH was added to both samples. To verify protein stability, 70 μM NADH was added again after about 35 min.

expressing 6XHisTag-FLVB and StrepIITag-FLVA were used to purify FLVA/FLVB complexes by two subsequent steps of immobilized metal affinity and Strep-Trap chromatography (Fig. S5*A*). SDS-page showed the presence of two bands in the fractions eluted from the second purification column (Figs. 5*A* and S5, *B–F*). Immunoblot analysis confirmed the presence of both FLVA and FLVB that were successfully co-purified (Figs. 5*A* and S5), demonstrating that FLVA and FLVB indeed form a heterotetramer stable enough to survive purification (Fig. S5*G*). Coomassie staining revealed a similar signal for the two proteins, suggesting a stochiometric ratio between FLVA and FLVB (Fig. 5*A*). UV visible absorption spectrum of FLVA/B preparations showed the presence of flavin typical peaks (373 nm, 450 nm) that were present also in FLVA and FLVB when expressed separately (Fig. 5*B*). About one molecule of FMN and Iron per FLV monomer were associated to FLVA/FLVB complexes, similarly to what was observed for FLVA/B alone (Table S2). The FLVA/B heterocomplex was also shown to be able to oxidize NADH and NADPH, exhibiting higher efficiency in the presence of NADH than NADPH (Fig. 5*C*). When FLVA/B was tested with different concentrations of NADH, the reactions fitted the steady state Hill equation (Fig. 5*D*), with a K′ of 51 ± 9 and Hill coefficient higher than 1, indicating cooperative binding of NADH to FLVA/B (Table 2).

Flavodiiron proteins complex formation requires intermolecular disulfide bonds

Mature FLVA and FLVB sequences contain respectively 16 and nine cysteine residues that may impact protein activity as it is the case for other stromal enzymes like some of the Calvin-Benson Cycle (31). We examined the influence of the redox state on recombinant FLVA/B complexes by subjecting them to treatment with or without DTT as a reducing agent prior to SDS-PAGE analysis. In the absence of DTT, FLVA/B formed heterotetrametric complexes that remained intact during separation on SDS-PAGE (Fig. 6*A*) and after size exclusion chromatography (Fig. S5). Exposure to DTT prompted the dissociation of FLVA/B heterocomplexes into monomers (Fig. 6*A*), indicating the presence of intermolecular disulfide bridges crucial for complex formation. Interestingly, both FLVA and FLVB exhibited similar behavior, forming homocomplexes under oxidizing conditions (Fig. S6). We next investigated enzymatic activity of purified FLVA/B when exposed to reducing conditions. Purified FLVs were incubated with DTT for 1 h before testing their catalytic activity. Interestingly we observed a severe decrease in the enzyme efficiency suggesting that FLVs activity is drastically altered in reducing conditions (Fig. 6*B*).

Discussion

Expression of active recombinant eukaryotic FLVs including all cofactors

While various studies have explored the functional role of FLVs in living organisms (13, 27, 28), there is a lack of information about their structural architecture and biochemical properties. To address this limitation, the present work investigated the biochemical and structural features of FLVs of a eukaryotic photosynthetic organism. *P. patens* FLVA, FLVB, and FLVA/B heterocomplexes expressed and purified from *E. coli* showed the expected molecular weight and bound flavin and iron atoms, as expected from the sequence analysis. Here, recombinant proteins were shown to be capable of reducing O_2 using NAD(P)H as electron donors, demonstrating that all the FLV proteins analyzed are active and properly folded when expressed in bacteria.

The iron coordination sites in the FLVB sequence revealed a type 1 canonical binding pattern characterized by Asp/Glu/His-rich residues (32). In contrast, FLVA is categorized as a type 2 protein, where the canonical diiron binding sites are substituted with neutral and basic residues (33). This peculiar amino acid composition in the diiron pocket domain raised some doubts about its ability to coordinate iron (23). In fact, the analysis of *Synechocystis* sp. PCC6803 Flv1, an orthologue of FLVA, presented conflicting information since the partial crystal structure of Flv1 revealed no iron (21), while the full-length recombinant Flv1 was found to bind iron (18). The data on recombinant *P. patens* FLVA suggest that despite possessing a non-canonical binding site, this protein is capable of coordinating iron. The type 2 binding site is a common occurrence in FLVs of photosynthetic organisms, indicating that having two isoforms with distinct properties in the iron-binding site is likely one of their conserved features. The distinct properties of the iron binding sites may correlate with the observed higher catalytic activity in FLVB as compared to both FLVA and the FLVA/B heterocomplex.

Here, FLV was shown to be active *in vitro* using NAD(P)H as electron donors, even if ferredoxin is expected to be the native electron donor of FLV based on deconvolution of

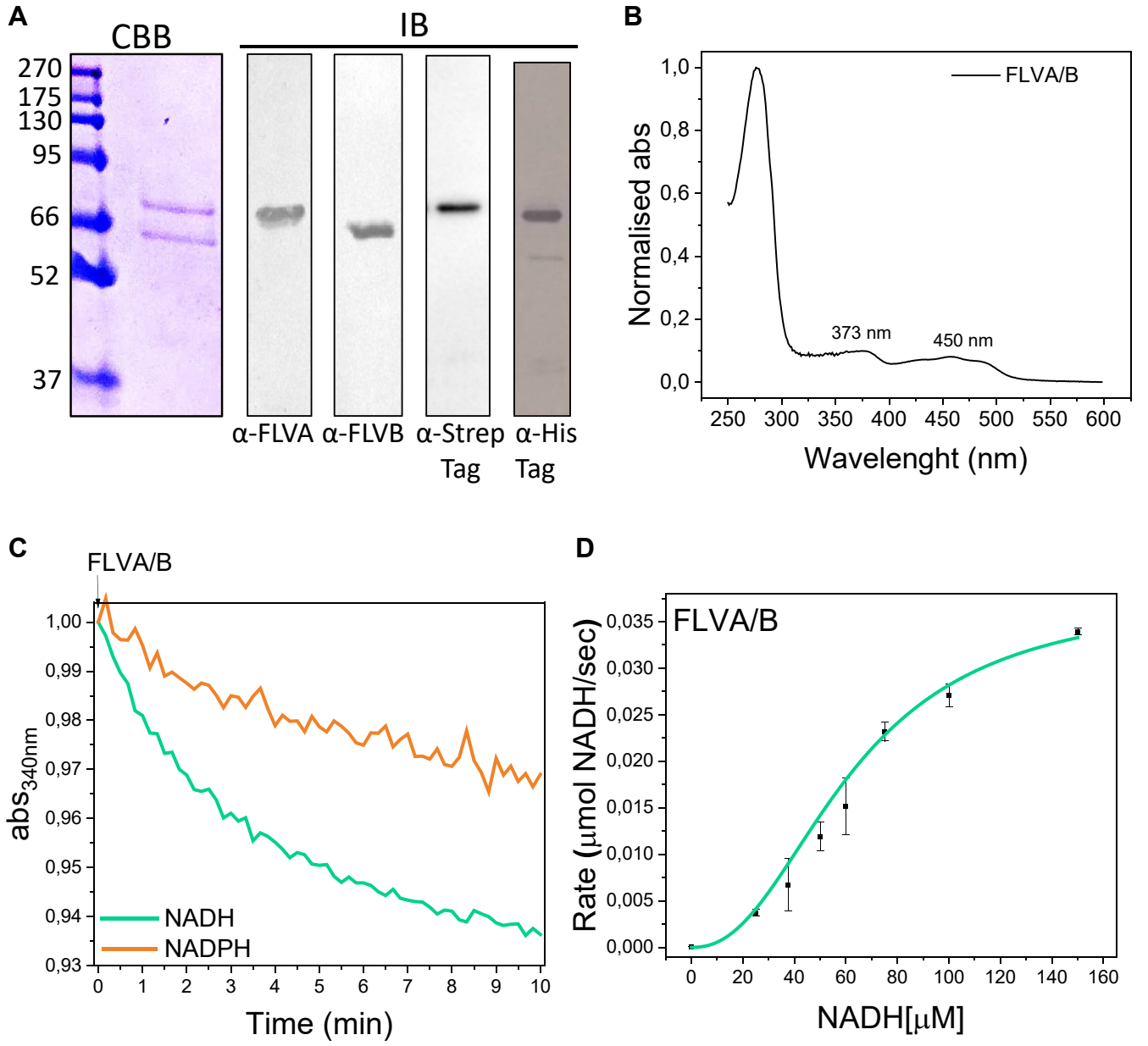

Figure 5. FLVA/FLVB heterocomplex biochemical and functional properties. *A*, representative Coomassie Brilliant Blue-stained SDS-polyacrylamide gel and Western blot analysis of purified heterocomplex using α-FLVA and α-FLVB, α-StrepTag, α-HisTag antibodies. On the left side, the apparent molecular weight of the ladder is reported in kDa. *B*, the absorption spectrum of approximately 5 µM FLVA/B in a solution containing 30 mM Tris and 300 mM NaCl at pH 8.0 was recorded at room temperature. *C*, NAD(P)H oxidase activity of 1 µM FLVA/B heterocomplex in the presence of 150 µM NADH (*green line*) and 150 µM NADPH (*orange line*). Traces were shifted to OD_{340nm} equal to 1 as the starting point immediately after protein adding. Absorption spectra were recorded at room temperature. *D*, Hill fitting Kinetics and fitted values for purified FLVA/B in the presence of NADH. The *solid line* indicates the Hill fitting curve. n = 3 Values are expressed ± SEM.

near-infrared spectroscopy signals of WT and *Δflv1/3* strains of *Synechocystis* sp. PCC6803 (19). A similar activity was also observed for the recombinant *Synechocystis* FLV where the electron transport from NAD(P)H was explained by an intramolecular electron transfer with the formation of reduced flavin intermediates (18). This suggests that the electron donation from NAD(P)H is possible, bypassing ferredoxins, at least *in vitro* for the isolated protein, as observed here.

Table 2
Hill kinetics of NADH oxidation for FLVA/B

Purified protein	K' (µM NADH)	V_{max} (µM NADH* s^{-1})	n (Hill coefficient)
FLVA/B	50.83 ± 8.88	0.03 ± 0.01	2.60 ± 0.40

Values were obtained from fits to the steady-state Hill equation. Three independent biological replicates were performed, values are expressed ± standard deviation.

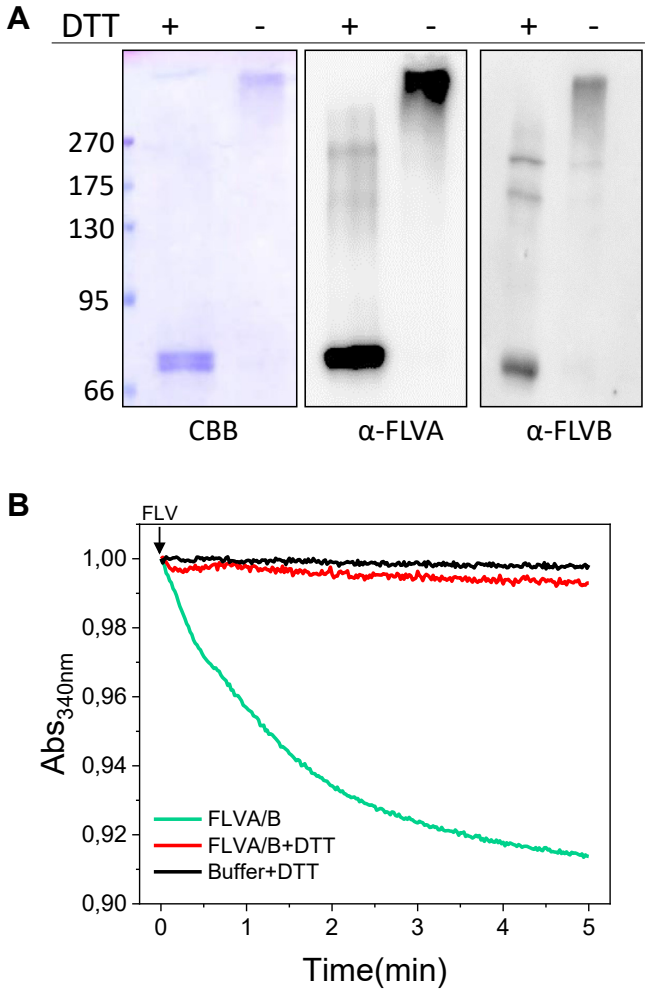

Figure 6. Redox dependence of flavodiiron proteins heterocomplex. *A*, SDS-PAGE and Western blotting of purified FLVA/B heterocomplex in the presence or absence of reducing agent. On the left side, the apparent molecular weight of the ladder is reported in kDa. The samples were incubated at room temperature in the presence or absence of DTT as indicated on the top of each lane. Prior to SDS-PAGE all samples were heated at 100 °C. *B*, FLVA/B heterocomplex NADH oxidase activity in the presence (*red line*) or absence (*green line*) of reducing agent. 4 μM of purified enzyme and the equivalent volume of protein buffer (*black line*) were incubated at room temperature for ∼1 h with DTT prior to activity test. 150 μM NADH without adding FLV and DTT was also monitored as a control (*black line*). Traces were shifted to OD_{340nm} equal to 1 as the starting point immediately after protein adding. Absorption spectra were recorded at room temperature.

In this context, it is interesting to observe that in a putative FLV catalytic cycle, hypothesized based on the available information on bacterial FDPs (34, 35) (Fig. 7*A*), four electrons are necessary for the complete reduction of O_2 to water. It is thus possible that *in vitro*, in the absence of Fdx, NAD(P)H is only capable of donating two. If this is the case, then the reaction *in vitro* would not be complete but only produce H_2O_2. Following this idea, the substrates NAD(P)H and O_2 would still be consumed, as experimentally observed, but the reaction would not be complete to water. Recombinant FDP of the anaerobic bacterium *Syntrophomonas wolfei* was indeed shown to produce H_2O_2 under certain conditions (36), showing that this is a realistic scenario also for FLVA/B.

This hypothesis also opens the possibility that *in vivo* two-electron donors, both Fdx and NAD(P)H, could both be involved in providing the four electrons required for the full FLV reaction (Fig. 7*B*) (19). This would be faster and with less accumulation of intermediate states with respect to the possibility that four electrons are all donated by a one-electron transporter such as Fdx, that would require four cycles of reduction oxidation. Plastid terminal oxidase PTOX, a non-heme diiron carboxylate enzyme, reduces O_2 to H_2O using plastoquinol as substrate. Depending on the substrate concentration, this enzyme has been shown to produce ROS probably from peroxo intermediates of the Fe center (37). Similar reactions may take place in the FLV catalytic cycle.

The hypothesis that NAD(P)H could also contribute as an electron donor would also be interesting since recombinant FLV proteins showed lower activity in the presence of NADPH as compared to NADH (38, 39). Such a low affinity for NADPH implies that when other pathways consuming reducing power are active, such as carbon fixation, would outcompete FLV for electron donors and FLV would be active only in case of electrons excess. Since the FLV reaction represents an energy loss, this kind of regulation would be beneficial since its activity should be present only when needed and minimized when other pathways are active.

FLVs form heterotetrametric complexes stabilized by disulfide bridges

In the genomes of photosynthetic organisms, FLVs are always found in pairs. In cyanobacteria, algae, and *P. patens*, the depletion of one protein results in the destabilization of the other, leading to the loss of all *in vivo* activity (8, 11, 13). In cyanobacteria, the overexpression of Flv3 in a *Δflv1* mutant background led to protein accumulation but proved insufficient for complete functional complementation (25). Furthermore, recent studies showed that *P. patens* FLVs are functional in angiosperms when the two enzymes are expressed together (27, 28).

In this study, we successfully isolated stable recombinant FLVA/B heterocomplexes using orthogonal purification and two different affinity tags. This demonstrated the strong interaction and ability of the two enzymes to form a heterocomplex where the two proteins are found in stoichiometric amounts. The FLVA/B complex was shown to be folded and exhibited enzymatic functionality in NAD(P)H oxidase activity. Notably, the overall activity of the heterocomplex was not higher than that of FLVB expressed alone. The potential advantage of having two distinct proteins is therefore likely not to enhance activity but to contribute to other features, such as regulation. This is consistent with the observed cooperativity of substrate binding to FLVs that is consistent with the formation of multisubunit complex FLVA/B heterocomplex.

Based on the *in vivo* observation of mutant plants (13), it was surprising to see that recombinant FLVA and FLVB form enzymatically active homotetramers even when expressed alone. The apparent contrast with *in vivo* observations can be attributed to differences in translation control between

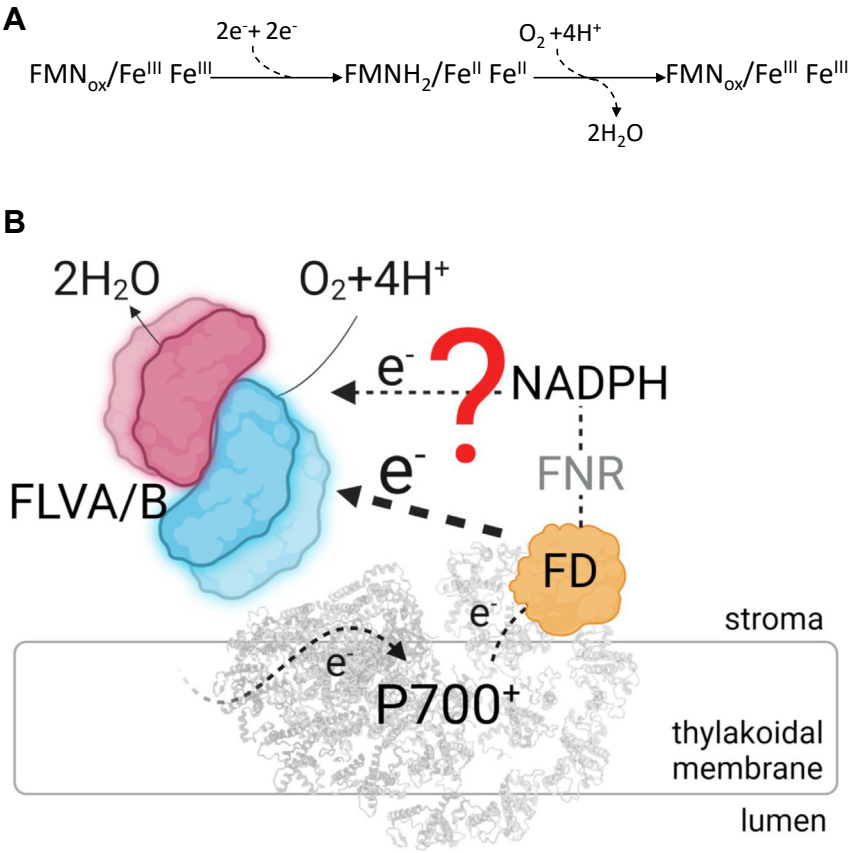

Figure 7. Proposed model describing *P. patens* flavodiiron protein catalytic activity. *A*, overall proposed reaction scheme. Four electrons are necessary for the complete reduction of O_2 to water, two electrons reduce the FMN moiety, while the other two the Fe-Fe center. *B*, FLVA and FLVB form stable bound heterotetramer in the stroma of *P. patens* chloroplasts. The *dashed line* indicates electron flow. Electrons coming from Fd and NADPH pool could participate in FLV oxygen reduction reaction.

prokaryotes and plant cells where homocomplexes are likely recognized and degraded. Nevertheless, this demonstrates that FLVA and FLVB are similar enough to enable the formation of a stable and active complex.

It is noteworthy that the FLVA/B heterocomplex is stabilized by intermolecular cysteine bridges that persist through protein denaturation but can be dissociated into monomers upon incubation in reducing conditions. Upon reduction, FLV activity is also decreased, possibly due to a direct effect on the intramolecular electron transport or as an indirect consequence of heterocomplex disassembly. It is well-established that proteins in the stroma, particularly enzymes of the CBB cycle, are regulated by the change of reducing potential when chloroplasts are illuminated. A similar regulation could also work for FLVs ensuring FLVs activity only when needed.

Experimental procedures

FLVA and FLVB sequence and structural analysis

P. patens FLVA (UniProtKB A9RYP3, Gene PHYPA_018517) and FLVB (UniProtKB A9RQ00, Gene PHYPA_001217) sequences were aligned with MUSCLE alignment of MAFFT Multiple Sequence Alignment and secondary structures were predicted with JNet prediction tool. Results were visualized and analyzed with JalView. FLVA and FLVB structural domains were annotated from PROFILE database (PS50902) and from the SMART database (SM00903). Model of FLVA and FLVB tertiary structures released by AlphaFold database (40) were also analyzed and visualized with PyMOL software. To investigate residues and predicted structures conservation *Synechocystis* sp. *PCC6803* Flv1-ΔFlR (Uniprot P74373, PDB 60HC) was used as reference.

FLV expression in E. coli *cells*

P. patens FLVA and FLVB were expressed in their mature form, complete of the three domains typical of photosynthetic organisms. The N-terminal residues of putative chloroplast transit peptide were calculated with TargetP-2.0 (https://services.healthtech.dtu.dk/service.php?TargetP-2.0) and excluded from the expressed sequence. The CDS encoding FLVA (residues 55–723) was cloned into pETite C-His Kan Vector (Lucigen) downstream of a sequence for a Strep-tag II (WSHPQFEK) to generate the recombinant plasmid pFLVA. The CDS encoding FLVB (residues 64–647) was cloned into pETDuet-1 (Novagen) downstream of a sequence for a hexahistidine (6xHis) tag to generate the recombinant plasmid pFLVB. Primer sequences and a detailed cloning procedure are reported in Table S1. *E. coli T7 Shuffle* competent cells were

transformed with pFLVA and pFLVB. For the heterocomplex purification, *E. coli T7 Shuffle* was simultaneously transformed with both plasmids and then plated on of Luria Bertani Agar medium (5 g/L Yeast extract, 10 g/L Tryptone, 3 ml/1L NaOH 1M, 10 g/L NaCl, Bacto agar 4 g/L) containing specific antibiotics (50 μM kanamycin for FLVA, 100 μM ampicillin for FLVB and both kanamycin and ampicillin for FLVA/B). Colonies were pre-inoculated in 50 ml of Luria Bertani (5 g/L Yeast extract, 10 g/L Tryptone, 3 ml/1L NaOH 1M, 10 g/L NaCl) liquid medium O/N and the pre-inoculum was then inoculated in 1 L of Terrific Broth (23.6 g/L Yeast extract, 11.8 g/L Tryptone, 9.4 g/L K_2HPO_4, 2.2 g/L KH_2PO_4, 4 ml/L Glycerol liquid). Specific antibiotics were also added to the pre-inoculum and to the inoculum (kanamycin for FLVA, ampicillin for FLVB, kanamycin + ampicillin for FLVA/B). The growth rate was monitored by periodical OD_{600nm} measurements, riboflavin (Sigma-Aldrich) 50 μM and ammonium iron (II) sulfate (Mohr's salt, $(NH_4)_2Fe\ (SO_4)_2(H_2O)_6$) 50 μM were added to the culture at OD_{600nm} ∼0.6 to promote their loading into proteins. 1 mM of isopropyl-β-D-thiogalactopyranoside (IPTG) was added at OD_{600nm} ∼0.8 to induce FLVA and/or FLVB expression. Bacterial liquid culture was then grown O/N at 16 °C and 180 rpm. Cells were harvested by centrifugation at 20,000*g* for 20 min, at 4 °C.

FLV purification from E. coli *cells*

The harvested cells were resuspended in lysis buffer (30 mM Tris-HCl pH 8, 300 mM NaCl and 0.1% V/V Triton x-100) and sonicated in the presence of lysozyme and protease inhibitors. After ultracentrifugation at 40,000*g* for 30 min, at 4 °C, the soluble fraction was collected for chromatography procedures. The soluble fraction was loaded onto Strep-Trap chromatography column (FLVA) (IBA-Lifesciences) or onto Immobilized Metal Affinity Chromatography column (FLVB) (Sigma-Aldrich) equilibrated with 20 mM Tris-HCl pH 8.0 and a salt gradient of 300 mM NaCl. The fractions containing StrepII-Tag-FLVA or 6XHisTag-FLVB were eluted with 30mMTris and 300 mM NaCl (pH 8.0). In case of FLVA/B heterocomplex purification, the bacterial soluble fraction was firstly loaded onto IMAC column, and the eluted material was then loaded into Strep-Trap chromatography column. Procedures and buffers were the same described above. Fractions containing FLVA, FLVB and FLVA/B were analyzed by SDS-page and then concentrated by ultrafiltration (Sartorius, Vivaspin, 10 kDa cutoff). FLVA/B was then subjected to a final purification step *via* Superdex 200 Increase 3.2/300 size exclusion chromatography column (Cytiva). Analysis of different purification steps and quality of protein purifications were also assessed by Immunoblot analysis with custom-made α-FLVA, α-FLVB antibodies and commercial α-HisTag, α-StrepTag antibodies (Biorad). After transferring to the nitrocellulose membrane, proteins were visualized with either Horseradish Peroxidase (HRP, Agrisera #AS09-60s) or Alkaline Phosphatase-conjugated secondary antibody (Sigma, #A3562). Notably, FLVB purification showed the highest purification yield (∼50 μM FLVB/4 ml elution volume) while FLVA and FLVA/B purification yield was 6 times lower (∼8 μM FLVA/4 ml elution volume).

Determination of FLV biochemical properties

UV–visible absorption spectra of purified FLVs were recorded at room temperature with Agilent Cary 60 spectrophotometer. Proteins were diluted in Tris 30 mM, Nacl 300 mM, pH 8 solution before measurement. Protein concentration was determined considering the abs_{280nm} and ε = 76,320 $M^{-1}*cm^{-1}$ for FLVA, ε = 66,810 $M^{-1}*cm^{-1}$ for FLVB and ε = 71,565 $M^{-1}*cm^{-1}$ for FLVA/B. ε was determined from protein sequences using Expasy ProtParam tool. Flavin concentration of purified proteins was spectroscopically determined. Absorbance at 373 nm and ε = 12,500 $M^{-1}*cm^{-1}$ was considered for quantitative FMN measurements. The ratio of protein concentration, determined by absorbance at 280 nm, to FMN content, determined by absorbance at 373 nm, was used to describe the quantity of cofactor per monomer FLV, as shown in Tables S1 and S2. Iron content of purified FLV was also spectroscopically determined with a standard ferrozine assay (41). Briefly, 200 μl of each protein sample (5–10 μM) were added with 50 μl of hydrochloric acid 12M, followed by heating the mixture for 20 min at 90 °C. The mixture was centrifugated (16.000*g*/15 min), and the resulting supernatant was treated with 60 μl ammonium acetate ($NH_4CH_3CO_2$; oversaturated solution). After 10 min of incubation at room temperature, 10 μl ascorbic acid ($C_6H_8O_6$; 75 mM) was added, followed by another 10 min of incubation. Eventually, 50 μl of FerroZine 10 mM were added and after 30 min of incubation at room temperature, the absorption spectra of all samples were acquired. The presence of iron was estimated by measuring the absorbance between 450 and 750 nm. Purified FLV displayed the typical iron absorption peak at 562 nm, protein buffer was also used as negative control.

Determination of FLV catalytic activity

FLV catalytic activity was determined by spectroscopic analysis. The assay mixture contained FLVs and NAD(P)H in Tris 30 mM, NaCl 300 mM, pH 8. NAD(P)H concentration was monitored by measuring absorption spectra (200–400 nm) every 12 s to follow the decrease at 340 nm at room temperature. For reducing conditions, purified FLV were pre-incubated for 1 h with DTT 50 mM before NAD(P)H oxidation assay (42). An equivalent volume of buffer was incubated with DTT 50 mM as a negative control. All redox treatments were carried out in 30 mM Tris, 300 Mm NaCl, pH 8. To measure kinetic parameters, different concentrations of NADH were used to calculate the activity of 0.07 μM FLVB, 5 μM FLVA, 5 μM FLVA/B. The results were fitted to the steady-state Hill equation:

$$y = v_{max} * x^n \,/\, (K^n + x^n)$$

y = enzyme activity at specified NADH concentration (x). v_{max} = maximum reaction velocity. x = NADH molar

concentration. n = Hill coefficient. K' = Half saturation costant. While the K′ of all enzymes is maintained throughout time, the activity was strongly affected by freezing and time. Therefore, all the reported values for V_{max} referred to fresh purified preparation.

FLV oxygen consumption rates were measured by a respirometer at 25 °C (O2K respirometer Oroboros). Purified FLVB was used at a final concentration of ∼6 μM and incubated with ∼150 μM NADH in Tris 30 mM, NaCl 300 mM (2 ml final volume). Oxygen concentration level (nmol/ml) in the sealed chamber was recorded over time for 60 min at room temperature.

Immunoblot analysis of purified proteins in oxidizing and reducing conditions

FLV enzymes were purified under non-reducing conditions allowing the formation of regulatory disulfide bonds. About 1 μg of purified FLVA, FLVB, FLVA-FLVB were treated with sample buffer (Tris-HCl 125 Mm, pH 6.8; glycerol 30% (w/v); sodium dodecyl sulfate 9% (w/v); 0.04% (w/v) bromophenol blue). In reducing conditions dithiothreitol (100 mM) was also added to the sample buffer. Proteins were denatured at 100 °C for 1 min, centrifugation at 13.000*g* for 5 min and then loaded onto SDS-PAGE (10% or 12% acrylamide). Proteins were stained by Brilliant Blue Coomassie or transferred to nitrocellulose membranes (Pall Corporation) for immunodetection with custom-made α-FLVA, α-FLVB antibodies as described above.

Data availability

All data are contained within the manuscript.

Supporting information—This article contains supporting information.

Acknowledgments—The authors thank Stefano Liberi, Monica Chinellato, Elisa Barbazza and Lorenzo Iacobucci for FLV cloning and setting up FLV purification. The authors thank Anja Krieger-Liszkay for critical reading and insightful discussion about FLV activity and ROS production. The authors would like to acknowledge the use of ChatGPT3.5 to revise some part of the text. T. M. thanks Oroboros Instruments GmbH for their support with O2k-PhotoBiology.

Author contributions—C. B., E. T., and M. B. investigation; C. B. and A. A.writing–original draft; C. B., T. M., A. A. writing–review & editing; L. C. and A. A. supervision; T. M. and A. A. conceptualization.

Funding and additional information—A. A. acknowledges funding from MUR PRIN2022PNRR - IRONCROP (P2022ZXWLK). A. A. acknowledges the Italian Ministry of University and Research (project funded by the European Union - Next Generation EU: "PNRR Missione 4 Componente 2, "Dalla ricerca all'impresa", Investimento 1.4, Progetto CN00000033"). T. M. acknowledges the support from European Union H2020 Project No. 859770-NextGen-O2k.

Conflict of interest—The authors declare that they have no conflicts of interest with the contents of this article.

Abbreviations—The abbreviations used are: FLV, Flavodiiron proteins; FNR, Ferredoxin-$NADP^+$-Reductase; PSI, Photosystem I.

References

1. Takagi, D., Takumi, S., Hashiguchi, M., Sejima, T., and Miyake, C. (2016) Superoxide and singlet oxygen produced within the thylakoid membranes both cause photosystem I photoinhibition. *Plant Physiol.* **171**, 1626–1634
2. Sonoike, K., and Terashima, I. (1994) Mechanism of photosystem-I photoinhibition in leaves of Cucumis sativus L. *Planta.* **194**, 287–293
3. Tiwari, A., Mamedov, F., Grieco, M., Suorsa, M., Jajoo, A., Styring, S., *et al.* (2016) Photodamage of iron-sulphur clusters in photosystem I induces non-photochemical energy dissipation. *Nat. Plants* **2**, 16035
4. Lima-Melo, Y., Gollan, P. J., Tikkanen, M., Silveira, J. A. G., and Aro, E.-M. (2019) Consequences of photosystem-I damage and repair on photosynthesis and carbon use in Arabidopsis thaliana. *Plant J.* **97**, 1061–1072
5. Asada, K. (2000) The water-water cycle as alternative photon and electron sinks. *Philos. Trans. R. Soc. Lond. B Biol. Sci.* **355**, 1419–1431
6. Walker, B. J., Strand, D. D., Kramer, D. M., and Cousins, A. B. (2014) The response of cyclic electron flow around photosystem I to changes in photorespiration and nitrate assimilation. *Plant Physiol.* **165**, 453–462
7. Alboresi, A., Storti, M., and Morosinotto, T. (2019) Balancing protection and efficiency in the regulation of photosynthetic electron transport across plant evolution. *New Phytol.* **221**, 105–109
8. Helman, Y., Tchernov, D., Reinhold, L., Shibata, M., Ogawa, T., Schwarz, R., *et al.* (2003) Genes encoding A-type flavoproteins are essential for photoreduction of O2 in cyanobacteria. *Curr. Biol.* **13**, 230–235
9. Ermakova, M., Battchikova, N., Richaud, P., Leino, H., Kosourov, S., Isojärvi, J., *et al.* (2014) Heterocyst-specific flavodiiron protein Flv3B enables oxic diazotrophic growth of the filamentous cyanobacterium *Anabaena* sp. PCC 7120. *Proc. Natl. Acad. Sci. U. S. A.* **111**, 11205–11210
10. Santana-Sanchez, A., Solymosi, D., Mustila, H., Bersanini, L., Aro, E.-M., and Allahverdiyeva, Y. (2019) Flavodiiron proteins 1-to-4 function in versatile combinations in O2 photoreduction in cyanobacteria. *Elife* **8**, e45766
11. Chaux, F., Burlacot, A., Mekhalfi, M., Auroy, P., Blangy, S., Richaud, P., *et al.* (2017) Flavodiiron proteins promote fast and transient O2 photoreduction in Chlamydomonas. *Plant Physiol.* **174**, 1825–1836
12. Shimakawa, G., Ishizaki, K., Tsukamoto, S., Tanaka, M., Sejima, T., and Miyake, C. (2017) The liverwort, Marchantia, drives alternative electron flow using a flavodiiron protein to protect PSI. *Plant Physiol.* **173**, 1636–1647
13. Gerotto, C., Alboresi, A., Meneghesso, A., Jokel, M., Suorsa, M., Aro, E.-M., *et al.* (2016) Flavodiiron proteins act as safety valve for electrons in Physcomitrella patens. *Proc. Natl. Acad. Sci. U. S. A.* **113**, 12322–12327
14. Bag, P., Shutova, T., Shevela, D., Lihavainen, J., Nanda, S., Ivanov, A. G., *et al.* (2023) Flavodiiron-mediated O2 photoreduction at photosystem I acceptor-side provides photoprotection to conifer thylakoids in early spring. *Nat. Commun.* **14**, 3210
15. Folgosa, F., Martins, M. C., and Teixeira, M. (2018) Diversity and complexity of flavodiiron NO/O2 reductases. *FEMS Microbiol. Lett.* https://doi.org/10.1093/femsle/fnx267
16. Martins, M. C., Romão, C. V., Folgosa, F., Borges, P. T., Frazão, C., and Teixeira, M. (2019) How superoxide reductases and flavodiiron proteins combat oxidative stress in anaerobes. *Free Radic. Biol. Med.* **140**, 36–60
17. Vicente, J. B., Gomes, C. M., Wasserfallen, A., and Teixeira, M. (2002) Module fusion in an A-type flavoprotein from the cyanobacterium Synechocystis condenses a multiple-component pathway in a single polypeptide chain. *Biochem. Biophys. Res. Commun.* **294**, 82–87

18. Brown, K. A., Guo, Z., Tokmina-Lukaszewska, M., Scott, L. W., Lubner, C. E., Smolinski, S., *et al.* (2019) The oxygen reduction reaction catalyzed by Synechocystis sp. PCC 6803 flavodiiron proteins. *Sustainable Energy Fuels* **3**, 3191–3200
19. Sétif, P., Shimakawa, G., Krieger-Liszkay, A., and Miyake, C. (2020) Identification of the electron donor to flavodiiron proteins in Synechocystis sp. PCC 6803 by in vivo spectroscopy. *Biochim. Biophys. Acta Bioenerg.* **1861**, 148256
20. Jokel, M., Nagy, V., Tóth, S. Z., Kosourov, S., and Allahverdiyeva, Y. (2019) Elimination of the flavodiiron electron sink facilitates long-term H2 photoproduction in green algae. *Biotechnol. Biofuels* **12**, 280
21. Borges, P. T., Romão, C. V., Saraiva, L. M., Gonçalves, V. L., Carrondo, M. A., Teixeira, M., *et al.* (2019) Analysis of a new flavodiiron core structural arrangement in Flv1-ΔFlR protein from Synechocystis sp. PCC6803. *J. Struct. Biol.* **205**, 91–102
22. Allahverdiyeva, Y., Isojärvi, J., Zhang, P., and Aro, E.-M. (2015) Cyanobacterial oxygenic photosynthesis is protected by flavodiiron proteins. *Life (Basel)* **5**, 716–743
23. Alboresi, A., Storti, M., Cendron, L., and Morosinotto, T. (2019) Role and regulation of class-C flavodiiron proteins in photosynthetic organisms. *Biochem. J.* **476**, 2487–2498
24. Allahverdiyeva, Y., Ermakova, M., Eisenhut, M., Zhang, P., Richaud, P., Hagemann, M., *et al.* (2011) Interplay between flavodiiron proteins and photorespiration in Synechocystis sp. PCC 6803. *J. Biol. Chem.* **286**, 24007–24014
25. Allahverdiyeva, Y., Mustila, H., Ermakova, M., Bersanini, L., Richaud, P., Ajlani, G., *et al.* (2013) Flavodiiron proteins Flv1 and Flv3 enable cyanobacterial growth and photosynthesis under fluctuating light. *Proc. Natl. Acad. Sci. U. S. A.* **110**, 4111–4116
26. Shimakawa, G., Shoguchi, E., Burlacot, A., Ifuku, K., Che, Y., Kumazawa, M., *et al.* (2022) Coral symbionts evolved a functional polycistronic flavodiiron gene. *Photosynth. Res.* **151**, 113–124
27. Yamamoto, H., Takahashi, S., Badger, M. R., and Shikanai, T. (2016) Artificial remodelling of alternative electron flow by flavodiiron proteins in Arabidopsis. *Nat. Plants* **2**, 16012
28. Wada, S., Yamamoto, H., Suzuki, Y., Yamori, W., Shikanai, T., and Makino, A. (2018) Flavodiiron protein substitutes for cyclic electron flow without competing CO2 assimilation in rice. *Plant Physiol.* **176**, 1509–1518
29. Wasserfallen, A., Ragettli, S., Jouanneau, Y., and Leisinger, T. (1998) A family of flavoproteins in the domains Archaea and Bacteria. *Eur. J. Biochem.* **254**, 325–332
30. Folgosa, F., Martins, M. C., and Teixeira, M. (2018) The multidomain flavodiiron protein from Clostridium difficile 630 is an NADH:oxygen oxidoreductase. *Sci. Rep.* **8**, 10164
31. Gurrieri, L., Fermani, S., Zaffagnini, M., Sparla, F., and Trost, P. (2021) Calvin–Benson cycle regulation is getting complex. *Trends Plant Sci.* **26**, 898–912
32. Romão, C. V., Vicente, J. B., Borges, P. T., Victor, B. L., Lamosa, P., Silva, E., *et al.* (2016) Structure of Escherichia coli flavodiiron nitric oxide reductase. *J. Mol. Biol.* **428**, 4686–4707
33. Gonçalves, V. L., Saraiva, L. M., and Teixeira, M. (2011) Gene expression study of the flavodi-iron proteins from the cyanobacterium Synechocystis sp. PCC6803. *Biochem. Soc. Trans.* **39**, 216–218
34. Di Matteo, A., Scandurra, F. M., Testa, F., Forte, E., Sarti, P., Brunori, M., *et al.* (2008) The O2-scavenging flavodiiron protein in the human parasite Giardia intestinalis. *J. Biol. Chem.* **283**, 4061–4068
35. Frederick, R. E., Caranto, J. D., Masitas, C. A., Gebhardt, L. L., MacGowan, C. E., Limberger, R. J., *et al.* (2015) Dioxygen and nitric oxide scavenging by Treponema denticola flavodiiron protein: a mechanistic paradigm for catalysis. *J. Biol. Inorg. Chem.* **20**, 603–613
36. Martins, M. C., Alves, C. M., Teixeira, M., and Folgosa, F. (2024) The flavodiiron protein from Syntrophomonas wolfei has five domains and acts both as an NADH:O2 or an NADH:H2 O2 oxidoreductase. *FEBS J.* **291**, 1275–1294
37. Yu, Q., Feilke, K., Krieger-Liszkay, A., and Beyer, P. (2014) Functional and molecular characterization of plastid terminal oxidase from rice (Oryza sativa). *Biochim. Biophys. Acta* **1837**, 1284–1292
38. Tamoi, M., Miyazaki, T., Fukamizo, T., and Shigeoka, S. (2005) The Calvin cycle in cyanobacteria is regulated by CP12 *via* the NAD(H)/NADP(H) ratio under light/dark conditions. *Plant J.* **42**, 504–513
39. Heineke, D., Riens, B., Grosse, H., Hoferichter, P., Peter, U., Flügge, U.-I., *et al.* (1991) Redox transfer across the inner chloroplast envelope membrane 1. *Plant Physiol.* **95**, 1131–1137
40. Jumper, J., Evans, R., Pritzel, A., Green, T., Figurnov, M., Ronneberger, O., *et al.* (2021) Highly accurate protein structure prediction with AlphaFold. *Nature* **596**, 583–589
41. Stookey, L. L. (1970) Ferrozine—a new spectrophotometric reagent for iron. *Anal. Chem.* **42**, 779–781
42. Cardi, M., Zaffagnini, M., De Lillo, A., Castiglia, D., Chibani, K., Gualberto, J. M., *et al.* (2016) Plastidic P2 glucose-6P dehydrogenase from poplar is modulated by thioredoxin m-type: distinct roles of cysteine residues in redox regulation and NADPH inhibition. *Plant Sci.* **252**, 257–266